DISCRETE AND CONTINUOUS
DYNAMICAL SYSTEMS SERIES S
Volume **12**, Number **8**, December **2019**

doi:10.3934/dcdss.2019145

pp. **2279–2305**

SOLVING THE BABYLONIAN PROBLEM OF QUASIPERIODIC ROTATION RATES

Suddhasattwa Das *

Courant Institute of Mathematical Sciences, New York University
251 Mercer street
New York 10012, USA

Yoshitaka Saiki

Graduate School of Business Administration, Hitotsubashi University
2-1 Naka, Kunitachi, Tokyo 186-8601, Japan
and
JST PRESTO, 4-1-8 Honcho, Kawaguchi-shi, Saitama 332-0012, Japan
and
University of Maryland, College Park, MD 20742, USA

Evelyn Sander

Department of Mathematical Sciences, George Mason University, USA

James A. Yorke

University of Maryland, College Park, USA

Abstract. A trajectory $\theta_n := F^n(\theta_0), n = 0, 1, 2, \ldots$ is quasiperiodic if the trajectory lies on and is dense in some d-dimensional torus $\mathbb{T}^d$, and there is a choice of coordinates on $\mathbb{T}^d$ for which F has the form $F(\theta) = \theta + \rho \bmod 1$ for all $\theta \in \mathbb{T}^d$ and for some $\rho \in \mathbb{T}^d$. (For $d > 1$ we always interpret $\bmod 1$ as being applied to each coordinate.) There is an ancient literature on computing the three rotation rates for the Moon. However, for $d > 1$, the choice of coordinates that yields the form $F(\theta) = \theta + \rho \bmod 1$ is far from unique and the different choices yield a huge choice of coordinatizations $(\rho_1, \cdots, \rho_d)$ of ρ, and these coordinations are dense in $\mathbb{T}^d$. Therefore instead one defines the rotation rate ρ_ϕ (also called rotation rate) from the perspective of a map $\phi : T^d \to S^1$. This is in effect the approach taken by the Babylonians and we refer to this approach as the "Babylonian Problem": determining the rotation rate ρ_ϕ of the image of a torus trajectory – when the torus trajectory is projected onto a circle, i.e., determining ρ_ϕ from knowledge of $\phi(F^n(\theta))$. Of course ρ_ϕ depends on ϕ but does not depend on a choice of coordinates for $\mathbb{T}^d$. However, even in the case $d = 1$ there has been no general method for computing ρ_ϕ given only the sequence $\phi(\theta_n)$, though there is a literature dealing with special cases. Here we present our *Embedding continuation method* for general d for computing ρ_ϕ from the image $\phi(\theta_n)$ of a trajectory, and show examples for $d = 1$ and 2. The method is based on the Takens Embedding Theorem and the Birkhoff Ergodic Theorem.

2010 *Mathematics Subject Classification.* Primary: 58F15, 58F17; Secondary: 53C35.

Key words and phrases. Quasiperiodic, Birkhoff Ergodic Theorem, rotation number, rotation rate, Takens Embedding Theorem, circular planar restricted 3-body problem, CR3BP.

The second author is supported by JSPS KAKENHI grant 17K05360, JST PRESTO grant JPMJPR16E5. The third author was supported by NSF grant DMS-1407087. The fourth author is supported by USDA grants 2009-35205-05209 and 2008-04049.

* Corresponding author: S. Das.

1. **Introduction.** The goal of this paper is to show how to compute a rotation rate of a quasiperiodic discrete-time trajectory. We begin with a motivating historical example, followed by a broad overview of our approach to determining rotation rates.

Rotation rates and quasiperiodicity have been studied for millennia; namely, the Moon's orbit has three periods whose approximate values were found 2500 years ago by the Babylonians [10]. Although computation of the periods of the Moon is an easy problem today, we use it to give context to the problems we investigate. The Babylonians found that the periods of the Moon - measured relative to the distant stars - are approximately 27.3 days (the sidereal month), 8.85 years for the rotation of the apogee (the local maximum distance from the Earth), and 18.6 years for the rotation of the line of intersection of the Earth-Sun plane with the Moon-Earth plane. They also measured the variation in the speed of the Moon through the field of stars, and the speed is inversely correlated with the distance of the Moon. This information is useful in predicting eclipses of the Moon, which occur only when the Sun, Earth and Moon are sufficiently aligned to allow the Moon to pass through the shadow of the Earth. How they obtained their estimates is not fully understood but it was through years of observations of the trajectory of the Moon through the field of distant stars in the sky. In essence they viewed the Moon projected onto the two-dimensional space of distant stars. We too work with quasiperiodic motions which have been projected into one or two dimensions.

This Babylonian effort could be viewed as the first "big data problem". What is meant by "big" of course depends on the era. The data recording technology consisted of sun-dried clay tablets.

The Moon has three periods because the Moon's orbit is basically three-dimensionally quasiperiodic, traveling on a three-dimensional torus $\mathbb{T}^3$ that is embedded in six (position+velocity) dimensions. The torus is topologically the product of three circles, and the Moon's orbit has an (average) rotation rate – i.e. the reciprocal of the rotation period – for each of these circles. While the Moon's orbit has many intricacies, one can capture some of the subtleties by approximating the Sun-Earth-Moon system as three point masses using Newtonian gravitational laws. This leads to the study of the Moon's orbit as a circular restricted three-body problem (CR3BP) in which the Earth travels on a circle about the Sun and the Moon has negligible mass. Using rotating coordinates in which the Earth and Sun are fixed while the Moon moves in three-dimensions, the orbit can thus be approximated by the above mentioned three-dimensional torus $\mathbb{T}^3$ in $\mathbb{R}^6$. Such a model ignores several small factors including long-term tidal forces and the small influence of the other planets.

As another motivating example, the direction ϕ of Mars from the Earth (viewed against the backdrop of the fixed stars) does not change monotonically. Now imagine that exactly once each year the direction ϕ is determined. How do we determine the rotation rate of Mars compared with an Earth year from such data?

This paper considers quasiperiodicity in a setting more general than the Moon or Mars – though both give good illustrations of our setting. The general problem of determining rotation rates for discrete-time maps has been unsolved in full generality even for images of one-dimensional quasiperiodic maps. We note that one reason quasiperiodicity is important for typical dynamical systems is that it is conjectured that there are only three kinds of recurrent motion that are likely to be seen in a dynamical system: periodic orbits, chaotic orbits, and quasiperiodic orbits [20].

Quasiperiodicity defined. Let $\mathbb{T}^d$ be a d-dimensional torus. A quasiperiodic orbit is an orbit that is dense on a d-dimensional torus and such that there exists a choice of coordinates $\theta \in \mathbb{T}^d := [0,1]^d \bmod 1$ (where mod1 is applied to each coordinate) for the torus such that the dynamics on the orbit are given by the map

$$\theta_{n+1} := F(\theta_n) = \theta_n + \rho \bmod 1 \tag{1}$$

for some **rotation vector** $\rho \in \mathbb{T}^d$ where the coordinates ρ_i of the ρ are irrational and **rationally independent**, i.e. if a_k are rational numbers for $k = 1, \cdots, d$ for which $a_1\rho_1 + \cdots + a_d\rho_d = 0$, then $a_k = 0$ for all $k = 1, \cdots, d$. We will say such a rotation vector ρ is **irrational**.

Linear changes of coordinates.

Define $\bar{\theta} := A\theta$ where A is a **unimodular** transformation, that is, an invertible $d \times d$ matrix with integer coefficients. In these coordinates, Eq. 1 becomes

$$\bar{\theta}_{n+1} = \bar{\theta}_n + A\rho \bmod 1. \tag{2}$$

Note that ρ is irrational if and only if $A\rho$ is. Hence the irrationality of ρ is well defined.

When we began this project, we felt the goal of determining rotation rates would be to determine the coordinates ρ_k of ρ. But that makes sense only if we have a well-defined coordinate system on $\mathbb{T}^d$, which is unrealistic. In fact we show in Section 2.2, for a given irrational ρ the set of vectors $A\rho \bmod 1$ for all unimodular matrices A is dense in the unit torus $\mathbb{T}^d$. If for example we wanted to know the coordinates of the vector ρ with 30-digit precision, each 30-digit vector v in $\mathbb{T}^d$ would be valid; that is, there is a unimodular matrix A for which $A\rho$ is within 10^{-30} of v.

Hence, motivated by the Babylonian experience, we need a concept of a rotation rate that does not depend on the choice of coordinates for $\mathbb{T}^d$.

Starting with a quasiperiodic map $F : \mathbb{T}^d \to \mathbb{T}^d$ and a d-dimensional quasiperiodic orbit $\theta_n := F^n(\theta_0)$ on a torus $\mathbb{T}^d$ for some d. Assume we have a map $\phi : \mathbb{T}^d \to S^1$. We establish a new method for computing rotation rates from the image $\phi(\theta_n)$ of the trajectory. The map F might arise as a Poincaré return map, as is used for the planar circular restricted three-body problem (CR3BP), and ϕ_n is the angle of the image of the trajectory as measured from the perspective of some reference point.

Two one-dimensional examples in Section 3. Fig. 1 shows two maps γ from a circle to the complex plane. The quasiperiodic map on the unit circle is Eq. 1. We identify circle S^1 with the interval $[0,1)$. The rotation rate can be thought of as the average value of the angle Δ_n, for $n = 1, 2, \cdots$. The trouble is that while we can average real numbers, we cannot average points on a circle, and much of this paper describes how to get around this difficulty, replacing Δ_n by its "lift" $\hat{\Delta}_n \in \mathbb{R}$. Then the "average" is $\rho_\phi := \lim_{N\to\infty} \frac{\sum_1^N \hat{\Delta}_n}{N}$. Viewing $\hat{\Delta}$ as a function defined on the torus $\hat{\Delta} : \mathbb{T}^d \to \mathbb{R}$, we require that $\hat{\Delta}(\theta)$ is continuous in θ if it is to give a meaningful rotation rate. Prop. 1 establishes the existence of the rotation rate, as described here and in Eq. 7, leaving "only" the question of how to determine $\hat{\Delta}_n$ numerically.

The Babylonian Problem. One might imagine that our goal would be to compute ρ in Eq. 1 from whatever knowledge we could obtain about the torus $\mathbb{T}^d$. However even though the Babylonians did not know about three-dimensional

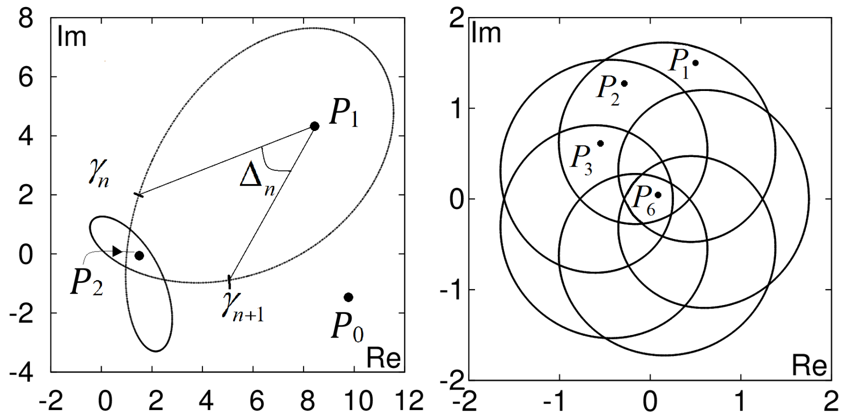

FIGURE 1. **The fish map (left) and flower map (right).** The function $\gamma : S^1 \to \mathbb{R}^2$ for each panel is respectively Eq. 21 and Eq. 22 and the image plotted is $\gamma(S^1)$ in the complex plane. These are images of quasiperiodic curves with self-intersections, and we want to compute the rotation rate only from knowledge of a trajectory $\gamma_n \in \mathbb{R}^2$. The curves winds j times around points P_j, so P_1 is a correct choice of reference point from which angles can be measured to compute a rotation rate. If instead we choose $j \neq 1$, then the measured rotation rate will be j times as big as for $j = 1$. In both cases, P_1 is the reference point. $P_1 = (8.25, 4.4)$ and $(0.5, 1.5)$ for the fish map and flower map, respectively. The angle marked $\Delta_n \in [0, 1)$ measured from point P_1 is the angle between trajectory points γ_n and γ_{n+1}. For each point γ_n we can define ϕ_n to be a unit vector $(\gamma_n - P_1)/\|\gamma_n - P_1\|$. Still using P_1, we can define a map $\phi : \mathbb{T}^d \to S^1$ - but since this is a one-dimensional torus, $\mathbb{T}^d = S^1$.

tori, they nonetheless obtained three meaningful rotation rates. To abstract their situation, we assume there is a smooth map $\psi : \mathbb{T}^d \to M$ where M is a manifold, usually of dimension 1 or 2. The **Babylonian Problem** is to compute a rotation rate ρ_ψ from knowledge of the projection of a trajectory. We assume we only have the values $\psi_n \in M$ of ψ at a sequence of times. We now describe the case where the manifold M is the circle S^1.

1.1. **Showing that the rotation rate ρ_ϕ is well defined. Notation for $\mathbb{T}^d$ and S^1 using** mod1**.** We will represent the circle S^1 as having a coordinate in $[0, 1)$. Hence $x \in S^1$ is a fraction of a revolution. The torus $\mathbb{T}^d = (S^1)^d$ is often represented as $\mathbb{R}^d/\mathbb{Z}^d$ but we require a representation with coordinates. Throughout this paper we consider $\mathbb{T}^d$ to be $[0, 1)^d$ mod 1, where each copy of $[0, 1)$ is the fraction of revolution around a circle. Furthermore $\theta \in \mathbb{T}^d$ can be treated as a set of d real numbers in $[0, 1)$. Similarly we can map $\mathbb{R} \to S^1$ by $x \mapsto x \bmod 1$. Of course write any $x \in \mathbb{R}$ unambiguously as

$$x = k + (x \bmod 1)$$

where k is the largest integer $\leq x$, and $(x \bmod 1)$ is the fractional part in $[0, 1)$.

What are the simplest maps of a torus to a circle?

Maps $\phi : \mathbb{T}^d \to S^1$ have a nice representation. Let $a = (a_1, \cdots, a_d)$ where $a_1, \cdots, a_d$ are integers and let $\theta = (\theta_1, \cdots, \theta_d) \in \mathbb{T}^d$. The simplest ϕ has the form $\phi_a(\theta) = a_1\theta_1 + \cdots + a_d\theta_d \bmod 1$. Then ϕ is a continuous map of the torus to a circle. Below we identify S^1 with the unit interval $\bmod 1$. For any initial point $\theta_0 \in \mathbb{T}^d$, let $\theta_n := F^n(\theta)$. Then $\phi_a(\theta_n) = \phi_a(\theta_0) + n(a_1\rho_1 + \cdots + a_d\rho_d) \bmod 1$ and in this very simple case $\phi_a(\theta_{n+1}) - \phi_a(\theta_n) = a \cdot \rho \bmod 1 := a_1\rho_1 + \cdots + a_d\rho_d \bmod 1$ is constant and in this very special case we obtain a constant rotation rate for $\phi = \phi_a$, namely

$$\rho_\phi \bmod 1 = (a \cdot \rho) \bmod 1. \tag{3}$$

See Eq. 8. For $d = 1$, Eq. 3 says $\rho_\phi = a_1\rho$ where a_1 is an integer. The integer a_1 depends on the choice of ϕ, so even when $|a_1| = 1$ we can get ρ for one choice and $-\rho$ for another choice by choosing $a_1 = \pm 1$.

A characterization of every map from torus to a circle. For every map ϕ of a torus to a circle, there are integers a_j and a function $g : \mathbb{T}^d \to \mathbb{R}$ such that

$$\phi(\theta) = g(\theta) + a \cdot \theta \bmod 1. \tag{4}$$

Computing a rotation rate for this map can be a bit difficult. In fact, after we define the rotation rate below, it will turn out that Eq. 3 will still be true, so the rotation rate will be independent of g. But this formula will not be very helpful in determining ρ_ϕ from the image of a trajectory, $\phi(\theta_n)$ since we do not know a and we do not have a coordinate system for the torus.

Defining the rotation rate ρ_ϕ as an "average".

We assume throughout this paper each continuous function such as those denoted by F, ϕ, γ, and ψ, and each manifold is smooth, by which we mean infinitely differentiable (denoted C^∞). This assures rapid convergence of our numerical methods.

Defining Δ and its lift $\hat{\Delta}$ for a projection $\phi : \mathbb{T}^d \to S^1$ to a circle. Rotation rates are key characteristics of any quasiperiodic trajectory. Suppose there exists a continuous map $\phi : \mathbb{T}^d \to S^1$ from the dynamical system to a circle, but we only know the image $\phi_n := \phi(n\rho)$ sequence of a trajectory $F(\theta_n) = \theta_{n+1} = \theta_n + \rho \bmod 1$ on a torus. Define

$$\begin{aligned}\Delta(\theta) &= \phi(\theta + \rho) - \phi(\theta) \bmod 1\\ &= g(\theta + \rho) + a \cdot (\theta + \rho) - [g(\theta) + a \cdot (\theta)] \bmod 1 \text{ (from Eq. 4)}\\ &= a \cdot \rho + g(\theta + \rho) - g(\theta) \bmod 1.\end{aligned} \tag{5}$$

We say $\hat{\Delta}$ is a **lift** of $\Delta : \mathbb{T}^d \to S^1$ if (i)$\hat{\Delta} : \mathbb{T}^d \to \mathbb{R}$, (ii) $\hat{\Delta}$ is continuous; and (iii) $\hat{\Delta}(\theta) \bmod 1 = \Delta(\theta)$. Motivated by Eq. 5, we define

$$\hat{\Delta}(\theta) := a \cdot \rho + g(\theta + \rho) - g(\theta). \tag{6}$$

Then (i),(ii), and (iii) are satisfied so $\hat{\Delta}$ is a lift of Δ.

Define $\hat{\Delta}_n = \hat{\Delta}(\theta_n)$. Define the **rotation rate** ρ_ϕ **for** ϕ of a quasiperiodic map F by

$$\rho_\phi := \left(\lim_{N\to\infty} \frac{\sum_{n=0}^{N-1} \hat{\Delta}_n}{N} \right) \bmod 1. \tag{7}$$

The following proposition says this definition is well defined.

Proposition 1. *Assume θ_n is quasiperiodic. Let $\hat{\Delta}_n := \hat{\Delta}(\theta_n)$ using Eq. 6. Then the limit in Eq. 7 exists and is the same for all initial θ_0. Using the notation of Eq. 4,*

$$\rho_\phi = a \cdot \rho \bmod 1. \tag{8}$$

Proof. The existence of the limit is guaranteed by the Birkhoff Ergodic Theorem (See Theorem 1.1), which says that the limit in Eq. 7 is

$$\int_{\mathbb{T}^d} \hat{\Delta}(\theta)d\theta = \int_{\mathbb{T}^d} \big(a \cdot \rho + g(\theta+\rho) - g(\theta)\big)d\theta$$

$$= a \cdot \rho + \int_{\mathbb{T}^d} g(\theta+\rho)d\theta - \int_{\mathbb{T}^d} g(\theta)d\theta \tag{9}$$

$$= a \cdot \rho, \tag{10}$$

since $\int_{\mathbb{T}^d} d\theta = 1$ and the two integrals in Eq. 9 are equal. Hence $\rho_\phi = a\cdot\rho \bmod 1$. □

Different choices of the lift $\hat{\Delta}$ can change the limit in Eq. 7 by an integer, but after applying mod1, the value of ρ_ϕ is independent of the choice of lift $\hat{\Delta}$.

A caveat. We note however, that in practice we do not know $a \cdot \rho$ so in practice we need to determine numerically what $\hat{\Delta}$ is and we must numerically evaluate the limit.

In the rest of this introduction, we give a non-technical summary of our results and a description of the standard tools that we use and finally a comparison to previous work on this topic. We then proceed with the technical aspects of the paper, in which we describe our methods and results in detail and give numerical examples for which we compute rotation rates.

1.2. **Where is the difficulty in solving the Babylonian Problem?** There are cases where it is easy to compute the rotation rate ρ_ϕ. If the angle always makes small positive increases, we can convert $\phi_{n+1} - \phi_n \bmod 1$ into a small real positive number in $[0, 1)$, and we can think of $\Delta_n = \phi_{n+1} - \phi_n$ as numbers in $(0, \alpha)$, where $0 < \alpha < 1$. The limit of the average of Δ_n is the rotation rate. The average of two or more angles in S^1 is not well defined. Hence we must average real numbers, not angles, and making that transition can be difficult.

Numerical determination of a lift $\hat{\Delta}$. The essential problem in computing ρ_ϕ is the determination of a lift $\hat{\Delta}$ for ϕ. Given a lift, we can compute ρ_ϕ using Eq. 7. While we know the fractional part of $\hat{\Delta}$ is $\Delta \in [0, 1)$, as we will explain later, we must choose the integer part k_n of each $\hat{\Delta}_n$ so that all of the points $(\theta_n, \hat{\Delta}_n) := (\theta_n, k_n + \Delta_n)$ lie on a connected curve in $S^1 \times \mathbb{R}$ (for $d = 1$) or a connected surface in in $\mathbb{T}^d \times \mathbb{R}$ (for $d > 1$). We must choose these integer parts despite the fact that we do not know which θ_n corresponds to Δ_n.

Even in that case $d = 1$ there has been no general method for computing the lift in order to find ρ_ϕ, though there is a literature dealing with special cases. See for example [2, 17, 16]. We have established a general method for determining the lift $\hat{\Delta}$, as summarized in the Figs. 1-5. Our method is based on the Theorem 1.2, a version of the Embedding Theorems of Whitney and Takens, described in detail in Section 2.

1.3. **Defining ϕ given either a map into $\mathbb{R}^2$ or $\mathbb{R}$.** Assume that we are given a planar projection $\gamma : \mathbb{T}^d \to \mathbb{R}^2$ and the images $\gamma(\theta_n)$. Fix a **reference point** $P \in \mathbb{R}^2$ that is not in the image $\gamma(\mathbb{T}^d)$. Let $\mathbb{R}^2$ be the complex plane $\mathbb{C}$, so that we can define $\phi(\theta) \in [0, 1) \bmod 1 = S^1$ by

$$e^{2\pi i\phi(\theta)} = \frac{\gamma(\theta) - P}{\|\gamma(\theta) - P\|}. \tag{11}$$

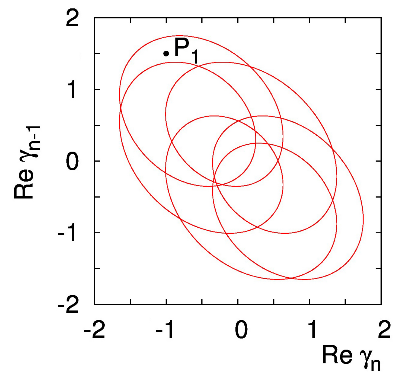

FIGURE 2. **The flower map revisited.** Suppose instead of having the function $\gamma : S^1 \to \mathbb{R}^2$ for the flower Eq. 22 in Fig. 1, we had only one coordinate of γ, for example, the real component, $Re\ \gamma$. Knowing only one coordinate would seem to be a huge handicap to measuring a rotation rate. But it is not. In the spirit of Takens's idea of delay coordinate embeddings explained in detail later, we plot $(Re\ \gamma_n, Re\ \gamma_{n-1})$ and choose a point P_1 as before, and the map is now two dimensional. The rotation rate can be computed as before. The rotation rate ρ_ϕ here using P_1 is the same as for Fig. 1 right.

The **winding number** around P is

$$W(P) := \int_0^1 \phi'(\theta + s)\, ds,$$

where $\phi' = \frac{d\phi}{dt}$. Note that $W(P)$ is an integral over the circle so it does not depend on θ. The value of W is piecewise constant and integer-valued. In our examples, it is critical that the projection of our quasiperiodic trajectory into $\mathbb{R}^2$ is such that there exists a point P in $\mathbb{R}^2$ with $|W(P)| = 1$. That is because the measured rotation rate will be higher by a factor of $|W(P)|$. For degenerate cases, there may be no point for which $|W(P)| = 1$, as shown in the next paragraph.

An example of a non-generic map γ. Consider the map given by $\gamma(z) = z^2$ where $z \in \mathbb{C}$. The map γ maps the unit circle onto the unit circle and for any value of $P \in \mathbb{C}$, $W(P) = 0$ if the reference point P is outside that circle, and $W(P) = 2$ if inside, and $W(P)$ is not defined if P is on the unit circle. Thus there is no point P such that $W(P) = 1$.

Two illustrative examples of complicated images of a quasiperiodic process. As mentioned earlier, Figure 1 shows the projections maps $\gamma : S^1 \to \mathbb{R}^2$, showing how the winding number differs in different connected components of the figure. On the left panel, every point inside the interior connected region that contains P_1 can act as a reference point for measuring angles and yields the same value of ρ_ϕ. If the map is sufficiently simple, (i.e., the nonlinearity g in Eq. 4 is sufficiently small), the rotation rate can immediately be computed as the average of these angle differences. However, if the map γ is more complicated, measurement of angle is compounded by overlap of lifts of the angle between two iterates, since they can be represented by multiple values (values differing by an integer).

Projections of $\mathbb{T}^d$ to $\mathbb{R}$. Sometimes we are only provided with a scalar-valued function $\gamma : \mathbb{T}^d \to \mathbb{R}$, and yet we can still construct a two-dimensional map and use the methods described for $\mathbb{R}^2$ projections. For example, Fig. 2 shows how we can recover a planar map from only the first component $Re\ \gamma_n$ of a flower map trajectory by considering planar points $(Re\ \gamma_{n-1}, Re\ \gamma_n)$. This map still gives same rotation rate as obtained by using the map in Fig. 1.

A similar example occurs with the Moon. The mean time between lunar apogees is 27.53 days, slightly longer than the 27.3-day sidereal month. Suppose we measure the distance D_n between the centers of the Earth and Moon once each sidereal month, $n = 0, 1, 2, \cdots$. Then the sequence D_n has an oscillation period of 8.85 years and can be measured using our approach by plotting D_{n-1} against D_n, and the point (D_{n-1}, D_n) oscillates around a point $P = (D_{av}, D_{av})$, where D_{av} is the average of the values D_n. Small changes in P have no effect on the rotation rate.

Yet another case arises from The Moon's orbit being tilted about 5 degrees from the Earth-Sun plane. The line of intersection where the Moon's orbit crosses the Earth-Sun plane precesses with a period of 18.6 years. The plane of the ecliptic is a path in the distant stars through which the planets travel. Measuring the Moon's angular distance from this plane once each sidereal month gives scalar time series with that period of 18.6 years. This example can be handled like the apogee example above.

As a last example, see also our treatment of the circular planar restricted three body problem in Section 4.2 where we compute two rotation rates of the lunar orbit, the first by plotting the rotation rate around a central point and the second by plotting $(r, dr/dt)$, deriving the rotation rate from a single variable $r(t)$, the distance from a central point, where t is time.

1.4. **The Birkhoff Ergodic Theorem.** We used the Birkhoff Ergodic Theorem to prove the existence of ρ_ϕ (Prop. 1) so now we must tell what that theorem says.

The Birkhoff Ergodic Theorem assumes there is an invariant set, which in our case is the set $\mathbb{T}^d$. Since we are interested here only in quasiperiodic dynamics, we can assume the dynamics are given by Eq. 1 where ρ is irrational. Lebesgue measure is invariant; that is, each measurable set E has the same measure as $F(E) = E + \rho$ and as $F^{-1}(E) = E - \rho$. This map is "ergodic" because if E is a set for which $E = F(E) = E + \rho$, then the measure of E is either 0 or 1.

The measure μ enables the computation of the space-average $\int_{\mathbb{T}^d} f d\mu$ for any L^1 function $f : \mathbb{T}^d \to \mathbb{R}$ when a time series is the only information available. Since μ is Lebesgue measure, we can rewrite that integral as $\int_{\mathbb{T}^d} f(\theta) d\theta$. We note that the Lebesgue measure of the entire torus is 1, so Lebesgue measure is a probability measure. Hence $\int_{\mathbb{T}^d} d\theta = 1$.

For a map $F : \mathbb{T}^d \to \mathbb{T}^d$, the **Birkhoff average** of a function $f : \mathbb{T}^d \to \mathbb{R}$ along the trajectory $\theta_n = F^n \theta_0$ is

$$B_N(f)(\theta_0) := \frac{1}{N} \sum_{n=0}^{N-1} f(\theta_n). \tag{12}$$

Theorem 1.1 (Quasiperiodic case of the Birkhoff Ergodic Theorem [3])**.** *Let $F : \mathbb{T}^d \to \mathbb{T}^d$ satisfy Eq. 1 where $\rho \in \mathbb{T}^d$ is irrational. Let μ be Lebesgue measure on $\mathbb{T}^d$. Then for every*[1] *initial $\theta_0 \in \mathbb{T}^d$, $\lim_{N\to\infty} B_N(f)(\theta_0)$ exists and equals $\int f d\mu$.*

[1]The ergodic theorem for general ergodic maps replaces "for every" with "for almost every" but for quasiperiodic maps the "almost" can be omitted.

1.5. **The method of weighted Birkhoff averages ($\mathbf{WB}_N^{[p]}$).** We have recently established a method for speeding up the convergence of the Birkhoff sum in Theorem 1.1 through introducing a C^∞ weighting function by orders of magnitude when the process is quasiperiodic and the function f is C^∞, a method we describe in [7, 6, 8]. In [8] it is proved that the limit of using $\mathrm{WB}_N^{[p]}$ is the same as Birkhoff's limit.

Weighted Birkhoff ($\mathrm{WB}_N^{[p]}$) average of f is calculated by

$$\mathrm{WB}_N^{[p]}(f)(\theta_0) := \sum_{n=0}^{N-1} \hat{w}_{n,N}^{[p]} f(\theta_n), \text{ where } \hat{w}_{n,N}^{[p]} = \frac{w^{[p]}(n/N)}{\sum_{j=0}^{N-1} w^{[p]}(j/N)}, \tag{13}$$

where the C^∞ weighting function w is chosen as

$$w^{[p]}(t) := \begin{cases} \exp\left(\dfrac{-1}{t^p(1-t)^p}\right), & \text{for } t \in (0,1) \\ 0, & \text{for } t \notin (0,1). \end{cases} \tag{14}$$

In our calculations of the rotation rates, we use $p = 1$ or 2. See in particular [7] for details and a discussion of how the method relates to other approaches. Note that essentially the same weight function as for $p = 1$ case is discussed by Laskar [15] in Remark 2 of the Annex, but he does not implement it.

1.6. **Delay coordinate embeddings.** For manifolds M_1 and M_2, a map $h : M_1 \to M_2$ is an **embedding** (of M_1) if h is a diffeomorphism of M_1 onto its image $h(M_1)$. In particular the map must be one-to-one.

Let $\psi : \mathbb{T}^d \to M_0$ be C^2 where M_0 is a smooth manifold of dimension D. In our applications below, ψ is either $\phi : \mathbb{T}^d \to S^1$ or $\gamma : \mathbb{T}^d \to \mathbb{R}^2$. While d is the dimension of the domain $\mathbb{T}^d$ of ψ, D is the dimension of the range.

For a positive integer K, define $\Theta_K^\psi : \mathbb{T}^d \to (M_0)^K$ as

$$\Theta(\theta) := \Theta_K^\psi(\theta) := \Big(\psi(\theta), \psi(F(\theta)), \cdots, \psi(F^{K-1}(\theta))\Big) \text{ for } \theta \in \mathbb{T}^d. \tag{15}$$

K is referred to as **the delay number** and is more precisely the number of coordinates used in defining Θ. See Discussion, Section 5. In the theorem below, if $K = 1$, we have a Whitney-type embedding theorem, or if $D = 1$, a Takens-like result.

In order to include both of the projection maps $\phi : \mathbb{T}^d \to S^1$ and $\gamma : \mathbb{T}^d \to \mathbb{R}^2$, we introduce the more general notation $\psi : \mathbb{T}^d \to M_0$, where the manifold M_0 is D-dimensional. Hence ϕ or γ can be substituted for ψ with $D = 1$ or 2, respectively.

Theorem 1.2. *[Special case of Theorem 2.5 in [21]] Let M_0 be a smooth D-dimensional manifold. Assume $F : \mathbb{T}^d \to \mathbb{T}^d$ is quasiperiodic where F is given in Eq. 1 and ρ is irrational. Assume*

$$2d + 1 \le KD.$$

Then for almost every C^2 function $\psi : \mathbb{T}^d \to M_0$, the map $\Theta : \mathbb{T}^d \to M_0^K$ is an embedding of $\mathbb{T}^d$.

While this result gives a lower bound on the delay number K, it is often convenient to choose K much larger than required.

Define $\Gamma = \Gamma_K^\psi : \mathbb{T}^d \to (M_0)^K \times \mathbb{R}$ as

$$\Gamma(\theta) := \Gamma_K^\psi(\theta) := (\Theta(\theta), \hat{\Delta}(\theta)) \text{ for } \theta \in \mathbb{T}^d. \tag{16}$$

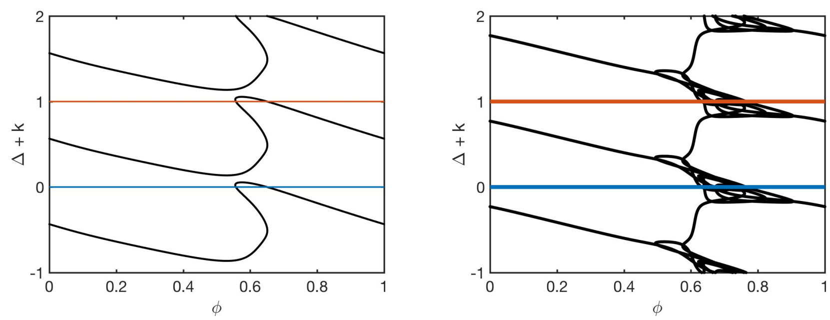

FIGURE 3. **The angle difference for the fish and the flower maps.** Here we plot $(\phi_n, \Delta_n + k)$ for every $n \in \mathbb{N}$ and all integers k, where $\Delta_n = \phi_{n+1} - \phi_n \bmod 1$. In the left panel (the fish map, the easy case) the closure of the figure resolves into disjoint sets (which are curves $\subset \mathbb{R} \times S^1$), while on the right (the flower map, the hard case) they do not. Hence if we choose a point plotted on the left panel, it lies on a unique connected curve that we can designate as $C \subset S^1 \times \mathbb{R}$. We can choose any such curve to define $\hat{\Delta}_n$, namely we define $\hat{\Delta}_n = \Delta_n + k$ where k is the unique integer for which $(\phi_n, \Delta_n + k) \in C$. A better method is needed to separate the set in the right panel into disjoint curves – and that is our embedding method.

where $\hat{\Delta}$ is given in Eq. 6. See Fig. 5. The following corollary follows immediately from Theorem 1.2.

Corollary 1. *Assume the hypotheses of Theorem 1.2. Then for almost every smooth (C^2) function $\psi : \mathbb{T}^d \to M_0$, the map $\Gamma_K^\psi : \mathbb{T}^d \to M_0^K \times \mathbb{R}$ is an embedding of $\mathbb{T}^d$.*

Theorem 2.1 explains how this result is used when we have the image of a trajectory such as $(\gamma(\theta_n))_{n=0}^{N-1}$ – when N is sufficiently large.

1.7. **Comparison to previous work.** We have written previously about computation of rotation rate in the papers [7, 6, 8]. A complete streamlined method for the case $d = 1$ is provided in Section 2; the Embedding continuation method is announced in [6], but this is the first paper in which it is explained. In addition, this paper is the first time that we have applied our methods to cases where $d > 1$. While we used the example (CR3BP) in [7], there we used a Poincaré return map whereas here in Section 4.2 no return map is used. We discuss the connections to our work with [2, 17, 16] in the subsequent sections of the paper. Those papers do investigate the Babylonian Problem, starting with only a set of iterates for a single finite length forward trajectory with the goal of finding a rotation number for some projection of a torus.

The investigation of quasiperiodic orbits is considered in [11, 5, 9, 13]. The approach in these papers assumes access to the full form of the original defining equations. Those papers are not investigating the Babylonian Problem.

Our paper proceeds as follows. We give a detailed description of our Embedding continuation method and an algorithm to implement it, in Section 2. Theorem

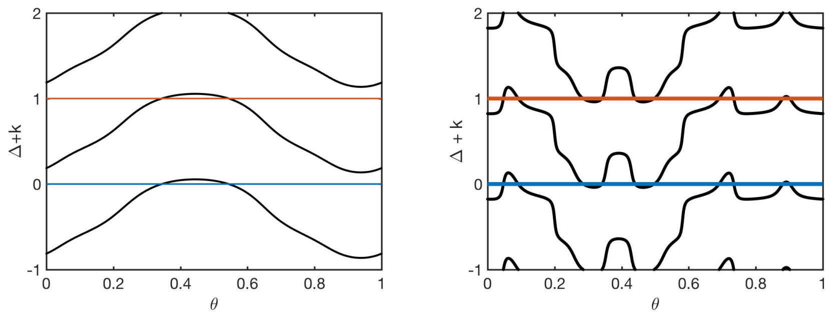

FIGURE 4. **A lift of the angle difference for the fish and for the flower maps.** This is similar to Fig. 3 except that the horizontal axis is θ instead of ϕ. That is, we take θ_n to be $n\rho$ and $\Delta(\theta) = \phi(\theta+\rho) - \phi(\theta) \bmod 1 \in [0,1)$ and we plot $(\theta_n, \Delta_n + k)$ for all integers k (where again $\Delta_n = \Delta(n\rho)$), These are points on the set $G = \{(\theta, \Delta(\theta)+k) : \theta \in S^1, k \in \mathbb{Z}\}$. This set G consists of a countable set of disjoint compact connected sets, "connected components", each of which is a vertical translate by an integer of every other component. For each $\theta \in S^1$ and $k \in \mathbb{Z}$ there is exactly one point $y \in [k, k+1)$ for which $\theta, y) \in G$. Each connected component of G is an acceptable candidate for $\hat{\Delta}$. Unlike the plots in Fig. 3, G always splits into disjoint curves. Unfortunately the available data, the sequence (ϕ_n) only lets us make plots like Fig. 3. But the Takens Embedding method allows us to plot something like G and determine the lift in the next figure.

2.1 gives a proof of convergence of our method. In Section 3, we illustrate our methods using two one-dimensional examples ($d = 1$). We refer to these as the *fish map* (introduced by Luque and Villanueva [16]) and the *flower map*, based on the shapes of the graphs. In Section 4 we give two-dimensional ($d = 2$) examples of maps for which we explore the difficulty of determining their rotation rates about a reference point. We end in Section 5 with a discussion.

2. **Embedding continuation method.** We have established that there is a lift $\hat{\Delta}$ of Δ and that Θ and $\Gamma_0 := \Gamma$ are embeddings of $\mathbb{T}^d$ for almost every ψ. **We will assume in this section that ψ has been chosen so that Θ and Γ_0 are embeddings.**

If we are given the image of a trajectory, either $\phi(\theta_n)$ or $\gamma(\theta_n)$, we do not yet know what the corresponding $\hat{\Delta}_n$ is. In this section, we describe how we find the lift of a map using our Embedding continuation method. A schematic of these ideas is depicted in Fig. 5.

A major difficulty in evaluating ρ_ϕ is that $\hat{\Delta}(\theta_n)$ is not known even though $\hat{\Delta}(\theta) \bmod 1 = \Delta(\theta)$. This is because $\hat{\Delta}(\theta) \in \mathbb{R}$ is a **lift** of $\Delta(\theta) \in S^1$; i.e., they differ by an (unknown) integer $m(\theta) := \hat{\Delta}(\theta) - \Delta(\theta)$. The key fact is that from its definition, $\hat{\Delta}(\theta)$ is continuous and since it is defined on a compact set it is uniformly continuous. We describe in Steps 1 and 2 below how to choose the integer part of

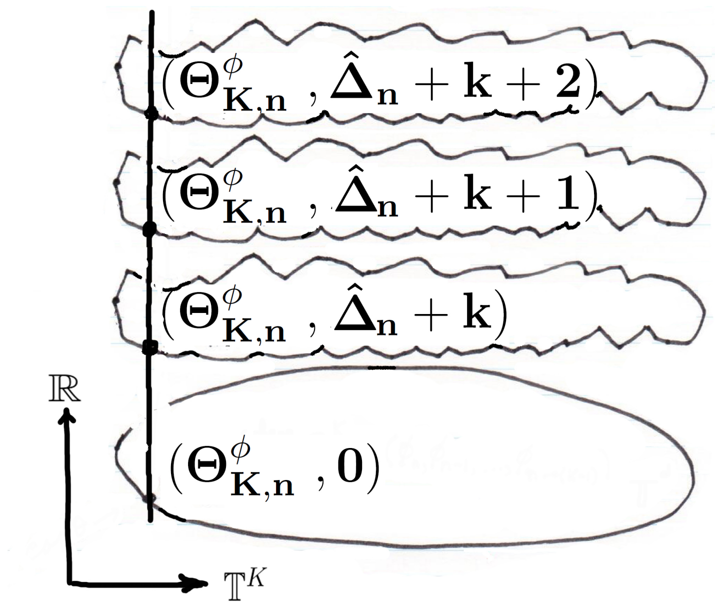

FIGURE 5. **Lifts over an embedded torus.** Let $\Theta := \Theta^{\phi}_K$ be as in Eq. 15 and let $\theta_n = n\rho$ be a trajectory on $\mathbb{T}^d$. Assume $K \geq 3$. By Theorem 1.2 for almost any map ϕ, the set $\Theta(\mathbb{T}^d)$ is an embedding of $\mathbb{T}^d$ into $\mathbb{T}^K$; i.e., Θ is a homeomorphism of $\mathbb{T}^d$ (the circle S^1 when $d = 1$) onto $\Theta(\mathbb{T}^d)$. In particular the map is one-to-one. The smooth (oval) curve is the set $(\Theta(\mathbb{T}^d), 0)$. As in our previous graphs, the vertical axis shows the angle difference $\Delta(\theta) \in [0,1)+k$ for all integers k. Write $\mathbb{U} := \{(\Theta(\theta), \Delta(\theta) + k) : \theta \in \mathbb{T}^d$ and $k \in \mathbb{Z}\}$. Unlike Fig. 3 but like Fig. 4, $\mathbb{U}$ always splits into bounded, connected component manifolds that are disjoint from each other. Hence $\mathbb{U}$, which is also the closure of the set $\{(\Theta(\theta_n), \Delta_n + k) : k \in \mathbb{Z}, n = 0, \cdots, \infty\}$, separates into disjoint components each of which is a lift of Δ and each of which is homeomorphic to $\mathbb{T}^d$. For each integer k the set $\{(\Theta(\theta), \Delta(\theta) + k) : \theta \in \mathbb{T}^d\}$ is a component as shown in this figure. See Theorem 2.1.

$\hat{\Delta}(\theta_n)$ consistently, that is, so that $\hat{\Delta}(\theta_n)$ is continuous on S^1. They collectively constitute our **Embedding continuation method**.

Step 1. The embedding. Let N be given; in practice we usually use $N \sim 10^5$ or 10^6 if $d = 1$. Choose the delay number K so that $2d + 1 \leq KD$. Recall that ψ is either γ or ψ in our applications. Since $\psi(\theta) \in M_0$, we have $\Theta(\theta) \in M_0^K$. By our version of the Takens Embedding Theorems, Theorem 1.2, if $2d + 1 \leq KD$, then for almost every smooth function ϕ, the map Θ is an embedding. In particular, there are no self intersections i.e., if $\Theta(\theta_1) = \Theta(\theta_2)$, then $\theta_1 = \theta_2$. That implies Γ defined by Eq. 16 is also an embedding of $\mathbb{T}^d$. We point out above that having an embedding guarantees that there are no self intersections, but there can be points far apart whose images are close to each other, and we try to avoid that by choosing K large.

Denote $\mathbb{U} = \{(\Theta(\theta), \Delta(\theta) + k) : \text{for all } \theta \in \mathbb{T}^d \text{ and all } k \in \mathbb{Z}\}$.

The minimum distance ϵ between components of $\mathbb{U}$. For each $j \in \mathbb{Z}$, define

$$\Gamma_j(\theta) = (\Theta(\theta), \hat{\Delta}(\theta) + j),$$

and write $\Gamma_j := \Gamma_j(\mathbb{T}^d)$. Of course $\Gamma_0 = \Gamma(\mathbb{T}^d)$. Then $\mathbb{U}$ is the union of all Γ_j. These sets are "vertical" translates of $\Gamma(\mathbb{T}^d)$ by an integer j, i.e. translates in the second coordinate. These are all disjoint from each other (since $\Theta(\mathbb{T}^d)$ is assumed to be an embedding). See Fig. 5 for an illustration.

Define

$$\epsilon := \inf\{\|p_1 - p_2\| : p_1, p_2 \in \mathbb{U} \text{ and are in different } \Gamma_j\}, \tag{17}$$

where $\|\cdot\|$ is the Euclidean norm on $\mathbb{R}^{2K+1}$.

Then $\epsilon > 0$ and ϵ is the minimum distance between points on different components of $\mathbb{U}$. In general ϵ is hard to compute from just the time series $\psi_n := \psi(\theta_n)$, so we have to fix a threshold $\delta > 0$, assuming that $\delta < \epsilon$. Then if $p_1, p_2 \in \mathbb{U}$ and $\|p_1 - p_2\| < \delta$, it follows that p_1 and p_2 are in the same component of $\mathbb{U}$.

The choice of the delay number K. It is important to note that this separation distance ϵ depends on the choice of K and we observe that increasing K increases ϵ, so that while Theorem 1.2 guarantees we have an embedding and therefore $\epsilon > 0$, this ϵ may be small. That might make it necessary to have a very large N, so instead we choose K much larger than the theorem requires.

Step 2. Extending by δ-continuation. Write $\Theta_n := \Theta(n\rho)$. The goal is to choose integers m_n so that all of the points $(\Theta_n, \Delta_n + m_n)$ for $n = 0, \cdots, N-1$ are in the same component. This may be impossible if N is not large enough. The point (Θ_0, Δ_0) is in some component and we choose $m_0 = 0$ which determines a component. Let $\mathbb{A}$ be the set of $n \in \{0, \cdots, N-1\}$ for which m_n has an assigned value. This set $\mathbb{A}$ changes as the calculation proceeds. Initially m_n is assigned only for $n = 0$ so at this point in the calculation the set $\mathbb{A}$ contains only 0. Each time we assign a value to some m_n, that subscript n becomes an element of $\mathbb{A}$. If there is an $n_1 \in \mathbb{A}$ and an $n_2 \notin \mathbb{A}$ and an integer k such that

$$\|(\Theta_{n_1}, \Delta_{n_1} + m_{n_1}) - (\Theta_{n_2}, \Delta_{n_2} + k)\| < \delta, \tag{18}$$

then the two points are in the same component and we assign $m_{n_2} = k$, which adds one element, n_2 to the set $\mathbb{A}$. Keep repeating this process (if possible) until all $\{m_n\}_{n=0}^{N-1}$ are assigned. (We will make this procedure precise in Prop. 2.)

For N sufficiently large, all can be assigned values, in which case we define $\hat{\Delta}_n = \Delta_n + m_n$ for all $n \in \{0, \cdots, N-1\}$. Define

$$\rho_\psi^N := \frac{\sum_{n=0}^{N-1} \hat{\Delta}_n}{N}.$$

In the following theorem, we want $\delta < \epsilon$ where ϵ is in Eq. 17.

Theorem 2.1. *For a d-quasiperiodic map assume Θ is an embedding. Given a map ψ, for δ sufficiently small, for all sufficiently large N (depending on δ), the above value ρ_ψ^N is well defined (since all m_n are defined), and*

$$\lim_{N\to\infty} \rho_\psi^N = \rho_\psi.$$

2.1. **Continuation algorithm: Long chains of little steps on $\mathbb{T}^d$.** To determine all $\hat{\Delta}(\theta_n)$ for all $n \in \{0, \cdots, n_{N-1}\}$, we begin knowing only $\hat{\Delta}(\theta_0)$. Knowledge of $\hat{\Delta}$ can spread like an infection, transmitted between nearby θ_n. The epidemic is spread only in little steps. The goal is to describe a continuation algorithm that identifies chains of n_j's starting from $n_j = 0$ and can reach every $n_j \in \{0, \cdots, n_{N-1}\}$.

To define "little step" we need a metric. Let $d(\cdot, \cdot)$ be a metric on $\mathbb{T}^d$ which is translation invariant, i.e. $d(x, y) = d(x + z, y + z)$ for all $x, y, z \in \mathbb{T}^d$. Furthermore for all $x = (x_1, \cdots, x_d)$ where all $|x_j| < 0.5$, let $d(x, 0) = \sum_j |x_j|$ (where here d denotes the distance on the "d"-dimensional torus).

According to Theorem 1.2, Θ is almost always an embedding of the (rigid-rotation) torus into a higher dimensional space, so we can reasonably assume the following hypothesis.

H_1. Θ is an embedding. (Hence Γ is also an embedding by Cor. 1.)

In this section we will assume ϵ is given by Eq. 17. Then $(\Theta, \hat{\Delta})(\mathbb{T}^d)$ is a smooth graph over $\Theta(\mathbb{T}^d)$. Hence if two points θ_1 and θ_2 in the are sufficiently close to each other, their images in $(\Theta, \hat{\Delta})(\mathbb{T}^d)$ will be less δ apart. That is given δ there is a $\delta_1 > 0$ such that $(d(\theta_{n_1}, \theta_{n_2}) < \delta_1)$ implies Ineq. 18 will be satisfied. Hence, if m_{n_1} has been assigned, and m_{n_2} has not, then we will now be able to assign it a value.

We say $(n_0, n_1, \cdots, n_k)$ is an N-δ_1-**chain** from θ_{n_0} to θ_{n_k} if $n_j \in \{0, \cdots, N-1\}$ for all $j \in \{0, \ldots, k-1\}$ and $d(\theta_{n_j}, \theta_{n_{j+1}}) < \delta_1$ for all $j \in \{0, \cdots, k-2\}$.

Proposition 2. (Long Chains of Little Steps). *Let $F : \mathbb{T}^d \to \mathbb{T}^d$ be the rigid rotation with rotation vector ρ with a dense trajectory. For $\delta_1 > 0$, there is $N > 0$ such that for every $n \in \{0, \cdots, N-1\}$ there is a N-δ_1-**chain** from θ_0 to θ_n.*

The following corollary interprets this proposition in terms of lifts and its proof is immediate.

Corollary 2. *Assume H_1. Assume $\delta_1 > 0$ is such that $d(\theta_{n_1}, \theta_{n_2}) < \delta_1$ implies Ineq. 18. Then, since $m_0 = 0$, all m_n can be determined. Write $\hat{\Delta}_j = \Delta_j + m_j$. Then all $\hat{\Delta}_j$ are in the same lift of Δ. In other words, $(\Theta^{\phi}_{K,j}, \hat{\Delta}_j)$ are all in the same component of $\mathbb{U}$ where $\mathbb{U}$ is defined in Fig. 5.*

To sketch a proof of the Proposition, we need the following fact. It is an elementary fact whose proof we leave to the reader.

Given $\delta_1 > 0$, there exists an N with the following property.

H_2. There exist integers $0 < \sigma_1 < \sigma_2 < \cdots < \sigma_P$ for some integer $P > 1$ that (i) the σ_j are relatively prime (i.e., the greatest common factor of all σ_j is 1) and (ii) θ_{σ_j} are within δ_1 of θ_0. Furthermore, $\sigma_1 + \sigma_P < N$.

It is always possible to choose N sufficiently large that $P = 2$ in H_2; however, we might not want to choose such a large N, and we might be satisfied with having $P > 2$.

An example of a pair θ_{σ_1} and θ_{σ_2} with relatively prime subscripts in dimension $d = 1$. The algorithm for creating chains does not depend on the dimension d. Here we let $d = 1$ and $\rho = \pi - 3$ and $N = 200$ and $\delta_1 = 0.01$ (where $d(0, x) = |x|$ for x close to 0). Then we can choose $\sigma_1 = 7$ and $\sigma_2 = 113$ since $\pi 7 - 22 \approx 0.008$ and $355 - \pi 113 \approx 0.00003$ so θ_7 and θ_{113} are within δ_1 of 0 and the subscripts 7 and 113 are relatively prime. We can reach every subscript in $\{0, \cdots, N-1\}$ by starting from 0 taking little steps, either increasing the subscript by 113 or decreasing it by 7, all the while staying between 0 and N, taking steps of size less than δ_1.

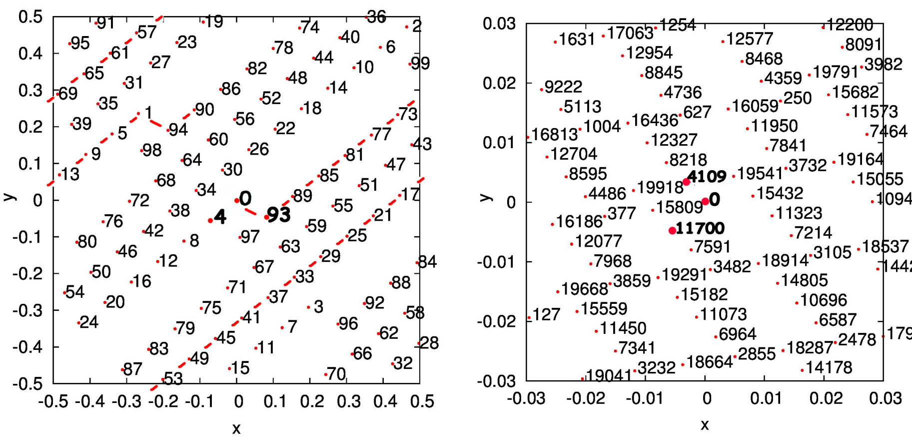

FIGURE 6. **Illustrating a chain of points on a rigid rotation on the torus.** $x_n = n\sqrt{3}$ (mod1), $y_n = n\sqrt{5}$ (mod1) for $n = 0, \cdots, N-1$ are plotted with the origin indicated by 0 at the center on the panel. Each point $\theta_n = (x_n, y_n)$ is labeled with its subscript n. Here $N = 100$ (left) and $= 20,000$ (right). Only the neighborhood of the origin is shown for the right panel. In the left panel, θ_4 and θ_{93} (i) are near the origin and (ii) their subscripts are relatively prime and (iii) the total of the subscripts is less than N. On the right points with subscripts 4109 and $11,700$ play the corresponding role. In each case it follows that there is a chain of points starting from 0 and ending at any desired θ_m where $0 < m < N$. This chain is a series of steps, each achieved by either adding one of the two subscripts or subtracting the other. See Prop. 2 and the algorithm sketched in its proof. In the left panel such a chain – adding 93 or subtracting 4 at each step – is shown that ends at θ_{90}.

An example of a pair θ_{σ_1} and θ_{σ_2} with relatively prime subscripts in dimension $d = 2$. See Fig. 6. On the left where $N = 100$, a chain is shown from 0 taking only steps of either $+93$ or -4. Both are within $\delta_1 = 0.13$ of 0. It would work equally well to take only steps of -93 or $+4$. When $N = 20,000$ on the right, there are two relatively prime subscripts 4109 and 11700 whose θ values are within $\delta_1 = 0.011$ of 0.

Proof of Proposition 2. We now describe why each θ_n can be reached by a chain starting from θ_0.

We assume that for the given δ_1, the N and σ_j have been chosen so that (i) and (ii) in H_2 are satisfied.

Let $B := B(\delta_1)$ denote the δ_1 neighborhood of $\theta_0 = 0$. First we assume the number P of σ_j satisfies $P = 2$, so θ_{σ_1} and θ_{σ_2} are in B and their subscripts are in $\{0, \cdots, N-1\}$ and are relatively prime.

For non-negative integers a_1, a_2, write

$$[[a_1, a_2]] := \theta_{a_2\sigma_2 - a_1\sigma_1} \in \mathbb{T}^d.$$

Suppose a_1 and a_2 are such that

$$0 \le a_2\sigma_2 - a_1\sigma_1 < N. \tag{19}$$

Since $0 \leq \sigma_1 + \sigma_2 < N$, we can either increase a_1 or a_2 by 1 (thereby decreasing $a_2\sigma_2 - a_1\sigma_1$ by σ_1 or increasing it by σ_2, respectively) and still have Condition 19 satisfied.

Notice that the distance from $[[a_1, a_2]]$ to $[[a_1 \pm 1, a_2]]$ or $[[a_1, a_2 \pm 1]]$ is less than δ_1. That is, changing either a_1 or a_2 by 1 moves $[[a_1, a_2]]$ by less than δ_1.

The key step of the proof is the following.

Algorithm for a chain. We choose a chain (see Fig. 6), which is a finite sequence (θ_j) of such points as follows, where each (θ_j) is of the form $[[a_1, a_2]]$. Our algorithm begins at θ_0 with $a_1 = a_2 = 0$.

A_1. Increase a_2 by 1 provided the subscript remains non negative; otherwise increase a_1 by 1. Repeat the process. Eventually the subscript returns to 0 (with $a_1 = \sigma_2$ and $a_2 = \sigma_1$. We have thereby created a chain of points on the torus, but we most likely have not encountered all the θ_j.

Next,

A_2. for each point in that chain, increase a_2 by 1, and repeat as long as Condition 19 satisfied. This process yields θ_n for every $n \in \{0, \cdots, N-1\}$.

If $P = 2$, we are done. When $P > 2$, the greatest common factor, denoted Ψ_2, of σ_1 and σ_2 is greater than 1. Then the above procedure reaches all points with subscripts divisible by Ψ_2 and no others. The next step is essentially the same as A_2 except that steps are taken by adding σ_3 to the subscript; that is,

A_3. Repeatedly add σ_3 to the subscript, as long as it remains less than N.

Taking all of those points and taking a small step for each by adding or subtracting σ_3 repeatedly will reach all points whose subscript is divisible by $\Psi_3 :=$ the greatest common divisor of σ_1, σ_2, and σ_3.

A_j. For each point that has been found so far, repeatedly add σ_j to the subscript as long as it remains less than N.

Eventually all θ_n for $0 < n < N$ will be reached. $\square$

2.2. A dense set of equivalent representations for each rotation vector.

While the definition of quasiperiodicity requires that the map has some coordinate system that turns the map into Eq. 1, that requirement by itself does not determine the coordinates of ρ. Fixing a coordinate system allows us to write $\rho = (\rho_1, \cdots, \rho_d)$ We have defined ρ in Eq. 1 in terms of a given coordinate system. Let $\bar{\theta} = A\theta$ where $\bar{\theta} \in \mathbb{T}^d$ and A is a unimodular transformation, that is an integer-entried matrix with determinant $|detA| = 1$, then in this new coordinate system Eq. 1 becomes

$$\bar{\theta} \mapsto \bar{\theta} + A\rho \bmod 1 \tag{20}$$

which is essentially Eq. 2. Hence $A\rho$ is also a rotation vector for the same torus map. Below we show we have a dense set of rotation vector representations.

Let $\mathcal{S}$ denote the set of integer-entried $d \times d$ matrices with determinant ± 1. Observe that for any $B \in \mathcal{S}$, $B^{-1} \in \mathcal{S}$. A matrix in $\mathcal{S}$ can be viewed as a change of variables on the torus, since it preserves volume. Therefore we call a vector $\tilde{\rho} \in \mathbb{R}^d$ a **rotation representation** of $\rho \in \mathbb{R}^d$ if $\tilde{\rho} = A\rho$ for some $A \in \mathcal{S}$. We ask: *When the vector ρ is irrational, what are all the possible rotation vectors (i.e., rotation representations), assuming $A \in \mathcal{S}$?*

Proposition 3. *Assume dimension $d \geq 2$. For an irrational rotation vector ρ, the set of its rotation vector representations is $S\rho$ (i.e., $\{A\rho : A \in S\}$), and $S\rho \bmod 1$ is dense in $\mathbb{T}^d$.*

Proof. To simplify notation we prove only the case of $d = 2$. The proof for $d > 2$ is analogous. See [12]. Write $\rho = (\rho_1, \rho_2)$. Note that the matrices $B_m := \begin{pmatrix} 1 & m \\ 0 & 1 \end{pmatrix}$ and $C_k := \begin{pmatrix} 1 & 0 \\ k & 1 \end{pmatrix}$ are in $\mathcal{S}$ for all integers m and k, as is $A := B_m C_k$. Then the vectors $(\rho_1, y_k) = C_k(\rho_1, \rho_2) \mod 1$ are *vertical* translates (translates in the direction $(0, 1)$) of $(\rho_1, \rho_2) \mod 1$, where $\{y_k\}$ is a dense set in S^1. When we similarly apply B_m for all m to each (ρ_1, y_k) we obtain a dense set of *horizontal* translates of (ρ_1, y_k) and thereby obtain a dense set in $\mathbb{T}^2$. Every coordinate of every point in that dense set is of the form $k_1\rho_1 + k_2\rho_2 \mod 1$ where k_1 and k_2 are integers. $\square$

3. **Examples of one-dimensional quasiperiodicity.** In this section, we give a detailed explanation of how we compute rotation rates for quasiperiodic maps on one-dimensional tori. For the first example computation of the rotation number is easy and straight forward while in the second it is sufficiently hard that we need our method. The pair of examples makes it clear when our method should be used.

One advantage of the examples below is that we know ρ and therefore we can compare it with the computed rotation rates.

Luque and Villanueva [16] addressed the case of a quasiperiodic planar curve $\gamma : S^1 \to \mathbb{C}$ and introduced what we call the *fish map*, depicted in the left panel of Fig. 1. Let

$$\gamma(\theta) := \hat{\gamma}_{-1} z^{-1} + \hat{\gamma}_0 + \hat{\gamma}_1 z + \hat{\gamma}_2 z^2, \tag{21}$$

where $z = z(\theta) := e^{i2\pi\theta}$ and $\hat{\gamma}_{-1} := 1.4 - 2i$, $\hat{\gamma}_0 := 4.1 + 1.34i$, $\hat{\gamma}_1 := -2 + 2.412i$, $\hat{\gamma}_2 := -2.5 - 1.752i$. (See Fig. 5 and Eq. 31 in [16]). They chose the rotation rate $\rho = (\sqrt{5} - 1)/2 \approx 0.618$ for the trajectory $\gamma_n = \gamma(n\rho)$ for $n = 0, 1, \cdots$ so we also use that ρ. The method in [16] requires a step of *unfolding* γ, which our method bypasses. We measure angles with respect to $P_1 = 8.25 + 4.4i$, where the winding number $|W(P_1)| = 1$.

Example 2. The flower map. We have created an example, the *flower map* in Fig. 1, right, to be more challenging than the fish. Let

$$\gamma_6(\theta) := (3/4)z + z^6 \text{ where } z = z(\theta) := e^{i2\pi\theta}. \tag{22}$$

We use the same $\rho = (\sqrt{5} - 1)/2$ as above. The choice of a reference point P_1 for which $|W(P_1)| = 1$ is shown in the right panel of Fig. 1. For our computations, we use $P = P_1 := 0.5 + 1.5i$. Points P_j with $|W(P_j)| = j$ for $j = 1, 2, 3, 6$ are also shown. For ρ_{γ_6}, the rotation rate of γ_6, to yield ρ or $1 - \rho \bmod 1$ is essential to choose a point P where $|W(P)| = 1$. In this example the values of Δ_n are dense in S^1, and $\max_\theta \hat{\Delta}(\theta) - \min_\theta \hat{\Delta}(\theta) \approx 1.2$.

For both examples, Fig. 1 shows two successive iterates γ_n and γ_{n+1}, and the angle Δ_n between these two iterates, computed with respect to a reference point P_1. It was computed by finding ϕ_n, the angle of γ_n with respect to P_1 as in Eq. 11. Using this, $\Delta_n = \phi_{n+1} - \phi_n \in [0, 1) \approx S^1$. On the left, in the fish map case, if we choose $\hat{\Delta}_0 := \Delta_0$ (or alternatively $:= \Delta_0 + m$ for some m), then we have selected the component in which all $\hat{\Delta}_n$ must lie. This is what is referred to below as *the easy case*. Choose some k, write $J_k := [a, b]$. Choose m_n is the integer for which $\Delta_n + m_n \in J_k$. It is not as easy to do this for the flower map on the right. Fig. 3 right shows that the possible lifts when plotted against ϕ form a tangled mess which does not resolve into bounded components, while when plotted against θ we obtain components that are diffeomorphic to S^1.

Figs. 3 and 4 show the possible lift values $\hat{\Delta}_n$ of the angle difference Δ_n plotted with respect to angle θ in Fig. 3 and ϕ in Fig. 4. For the fish map on the left, we see that we can set $[a, b] \approx [0.18 + k, 1.05 + k]$ for any integer k. Furthermore, we investigated the rotation rate of the signal viewed from $P_1 = 7 + 4i$. Using the Weighted Birkhoff Average, we observe that the deviations of the approximate rotation from ρ falls below 10^{-30} when the iteration number exceeds $N = 20,000$, and since we know the actual rotation rate, we can report that the error in the rotation rate is then below 10^{-30}. Once we have found a proper lift for the flower map, we can do the same procedure. The next section explains how we go about finding a lift in this more complicated case.

4. **Higher-dimensional quasiperiodic examples.** We develop a higher-dimensional method to compute the rotation vector ρ purely from knowledge of the sequence $\theta_{n+1} := F(\theta_n)$. The question of how to compute the rotation vector is actually two questions. Question 1: If we compute a rotation vector, what are the possible values? Question 2: How do we compute any of the possible values for the rotation vector in difficult cases? Figs 8, 9, and 10, demonstrate that like in one dimension, in d dimensions we are able to use d independent planar projections combined with a higher-dimensional version of our Embedding continuation method in order to find a lift, each projection leading to one component of a d-dimensional rotation vector. In fact, these rotation vectors are not unique. In this section, we give a detailed discussion of our higher-dimensional method, describing the possible values we can achieve in calculating a rotation vector. We then illustrate our method for three examples: the fish torus, the flower torus, and the restricted three-body problem.

4.1. **Two examples in a higher dimension: fish and flower tori $\mathbb{T}^2$.** We use the fish and flower maps from the previous section in order to create 2-dimensional torus maps. We will explore the problem of computing rotation rates for these examples where we know the rotation rates for the quasiperiodic maps. Let $\rho := (\sqrt{5} - 1)/2$ and $\phi := \sqrt{3}/2$, and define

$$(\theta_n, y_n) := (n\rho \mod 1, n\phi \mod 1) \in \mathbb{T}^2 \tag{23}$$

Let γ be either the fish or the flower map defined in the previous section. Define the torus-version f_T of the γ map(s) as follows. Let $Re(\cdot)$ and $Im(\cdot)$ denote the real and imaginary components of a complex number, and let $f_T : \mathbb{T}^2 \to \mathbb{R}^3$. Write $f_T(\theta_n, y_n) = (f_1, f_2, f_3)(\theta_n, y_n)$, where

$$f_1(\theta_n, y_n) = Re(\gamma(\theta_n) + 2)\cos(2\pi y_n) \tag{24}$$

$$f_2(\theta_n, y_n) = Re(\gamma(\theta_n) + 2)\sin(2\pi y_n) \tag{25}$$

$$f_3(\theta_n, y_n) = Im(\gamma(\theta_n)). \tag{26}$$

The "+2" is just for convenience so that the torus image can wrap around the origin rather than having to wrap it around some other point. For each γ, the map f_T takes a quasiperiodic trajectory into $\mathbb{R}^3$.

Two projections of a torus for two rotation rates. Figure 8 shows two independent projections of f_T to $\mathbb{R}^2$. For the first rotation rate, we project f_T to (f_1, f_2) in the plane. Then we measure the angle ϕ from a reference point P which is not in the image of the torus. In particular, $P = (0, 1.5)$ for the fish torus, and

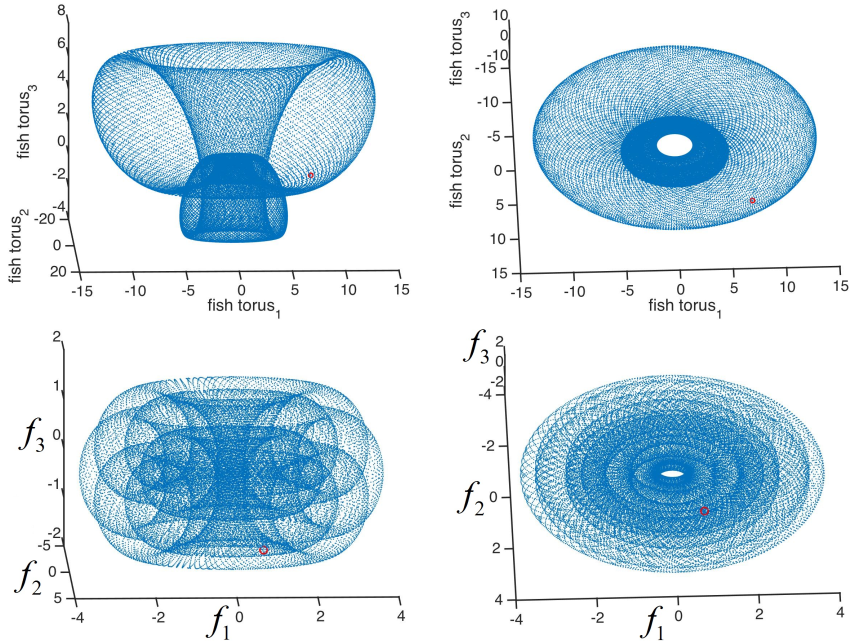

FIGURE 7. **The fish and flower torus.** The top figures show two views of the fish torus, and the bottom two views of the flower torus. These figures can be thought of as projections of tori onto the plane represented by the page. The three coordinate axes are presented here to clarify which two-dimensional projection is being used. The projections of the tori on the left are simply connected so there is no way to choose a point P that would yield a non-zero rotation rate. The projections on the right yield images of the tori that are annuli with a hole in which P can be chosen to yield non-zero results. Each is a plot of $N = 50090$ iterates. The red circle is the initial point.

$(0, 0.1)$ for the flower torus. For both maps, this projection gives a rotation rate of $\phi/2\pi$ (the denominator 2π comes from the fact that we are measuring angles in $[0, 1]$).

For a second rotation rate, let R_α be the rotation matrix that tilts by angle $\alpha = 0.05\pi$ in the $f_2 - f_3$ plane. Namely

$$R_\alpha = \begin{pmatrix} 1 & 0 & 0 \\ 0 & \cos\alpha & -\sin\alpha \\ 0 & \sin\alpha & \cos\alpha \end{pmatrix}$$

Set

$$h = R_{0.05\pi} f.$$

Define $r = \sqrt{h_1^2 + h_2^2}$. Then our projection is to the value (r, f_3). We measure the angle of this projection relative to the point $(8.25, 4.4)$ for the fish torus, and $(2.6, 1.4)$ for the flower torus. For both maps, this projection gives rotation rates of $1 - \phi/(2\pi)$ and $1 - \rho$. Why the tilt by 0.05π rather than use value of r with respect

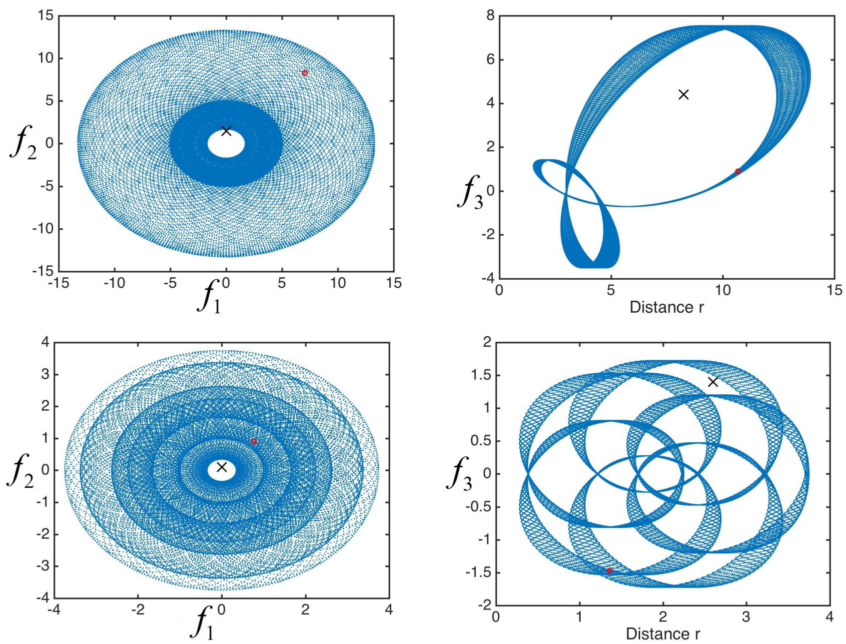

FIGURE 8. **Projections of the fish torus and the flower torus.** The coordinates used to find angle 1 (left) and angle 2 (right) for the fish torus (top) and the flower torus (bottom). The red circle shows the initial condition. The $\times$ shows the point with which the angle is measured. Note that for the the fish torus, the point from which the angle is measured is very close to the edge torus image. For angle 2, points are projected onto a tilted plane that makes angle 0.05π with the horizontal. See Section 4.1 for a full description of these projections.

to the original coordinates? Because without the tilt (i.e. $\alpha = 0$), the projection would be a curve rather than a thick strip, which would not give a true test of our Embedding continuation method in two dimensions.

In both cases, we get a map whose image has at least one hole (in which the winding number $= \pm 1$), and we can measure angles ϕ and angle differences Δ compared to a point inside one of the holes, as long as the torus has a winding number $|W(p)| = 1$ with respect to points in this hole. Thus just as for the one-dimensional case, we compute the lift, and then compute the rotation rate for these two different projections.

Figures 9 and 10 show the original values of the angle difference, and the computed lift, respectively. Note that fish torus lift is easy to compute while the flower torus requires and embedding.

As mentioned in Section 1, rather than using Birkhoff Averages, we achieve more rapid convergence using our Weighted Birkhoff Average, denoted $\mathrm{WB}_N^{[p]}$ in Eq.13. Define the ρ approximation $\rho_N := \mathrm{WB}_N^{[1]}(\hat{\Delta}_n)$, when $p = 1$. Fluctuations in ρ_N fall below 10^{-30} for $N > 20,000$. Since we know the actual rotation rate, we can report that the error $|\rho - \rho_N|$ is then below 10^{-30}.

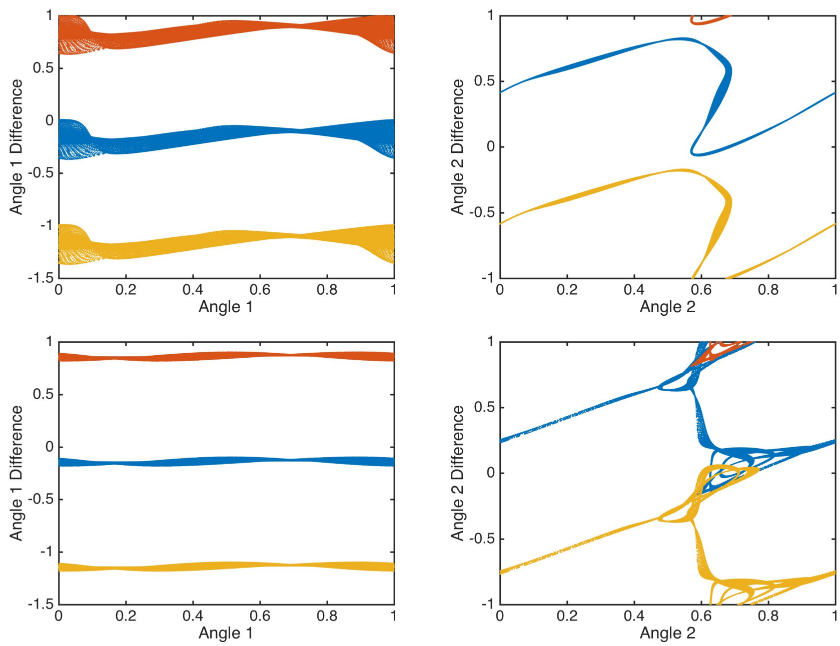

FIGURE 9. **Angle differences for the fish torus and flower torus.** Each panel shows three possible angle differences, each differing by an integer, for the same projections as were depicted in Fig. 8. The angle versus angle difference for angle 1 (left) and angle 2 (right) for the fish torus (top) and flower torus (bottom). In the final panel, the picture cannot be separated into separate components.

4.2. **The circular planar restricted three-body problem (CR3BP).** CR3BP is an idealized model of the motion of a planet, a moon, and an asteroid governed by Newtonian mechanics Poincaré [19, 1] introduced his method of return maps using this model. In particular, we consider a circular planar three-body problem consisting of two massive bodies ("planet" and a large "moon") moving in circles about their center of mass and a third body ("asteroid") whose mass is infinitesimal, having no effect on the dynamics of the other two.

This model can also (simplistically) represent the Sun-Earth-Moon system discussed in the introduction though the parameter μ has to be changed, and the Moon is the body that is assumed to have negligible mass. All three travel in a plane.

We assume that the moon has mass μ and the planet mass is $1-\mu$ where $\mu = 0.1$, and writing equations in rotating coordinates around the center of mass. Thus the planet remains fixed at $(q_1, p_1) = (-0.1, 0)$, and the moon is fixed at $(q_2, p_2) = (0.9, 0)$. In these coordinates, the satellite's location and velocity are given by the *generalized position vector* (q_1, q_2) and *generalized velocity vector* (p_1, p_2).

Define the distance of the asteroid from the moon and planet are

$$d_{moon}^{2} = (q_1 - 1 + \mu)^2 + q_2^2$$

$$d_{planet}^{2} = (q_1 + \mu)^2 + q_2^2.$$

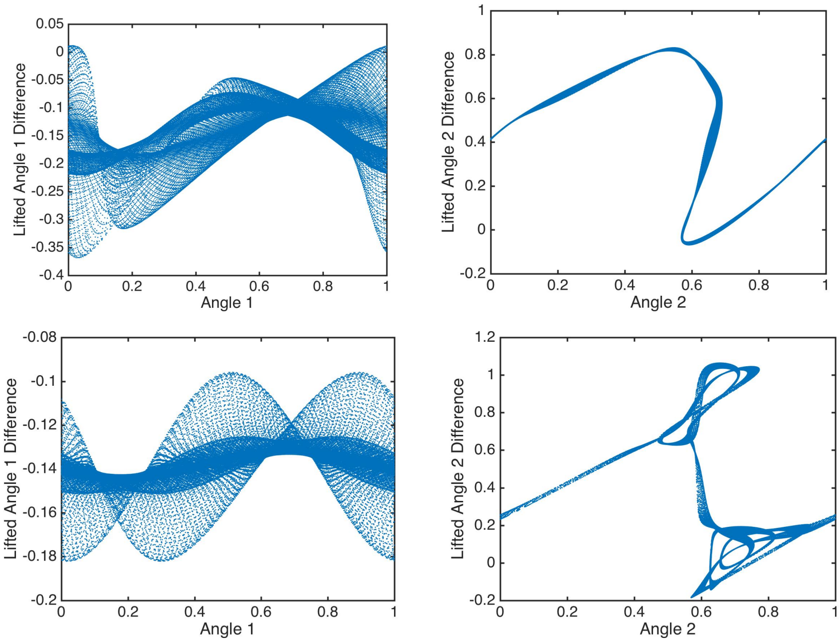

FIGURE 10. **Lifts of the angle difference for the fish torus and flower torus.** Here one of the possible lifts has been selected from each panel in Fig. 9. Each panel shows the angle versus angle difference lift for fish torus angle 1 (top left) and angle 2 (top right) and the flower torus angle 1 (bottom left) and angle 2 (bottom right), using the projections depicted in Fig. 8.

The following function H is a Hamiltonian (see [22] p.59 Eqs. 63-66) for this system

$$H = \frac{1}{2}(p_1^2 + p_2^2) + p_1 q_2 - p_2 q_1 - \frac{1-\mu}{d_{planet}} - \frac{\mu}{d_{moon}}, \tag{27}$$

where $p_1 = \dot{q_1} - q_2$ and $p_2 = \dot{q_2} + q_1$. We get the equations of motion from

$$\begin{aligned} \frac{dq_i}{dt} &= H_{p_i}, \\ \frac{dp_i}{dt} &= -H_{q_i}. \end{aligned}$$

That is, the equations of motion are as follows:

$$\begin{aligned} \frac{dq_1}{dt} &= p_1 + q_2, \\ \frac{dq_2}{dt} &= p_2 - q_1, \\ \frac{dp_1}{dt} &= p_2 - \mu\frac{q_1 - 1 + \mu}{d_{moon}^3} - (1-\mu)\frac{q_1 + \mu}{d_{planet}^3}, \\ \frac{dp_2}{dt} &= -p_1 - \mu\frac{q_2}{d_{moon}^3} - (1-\mu)\frac{q_2}{d_{planet}^3}, \end{aligned}$$

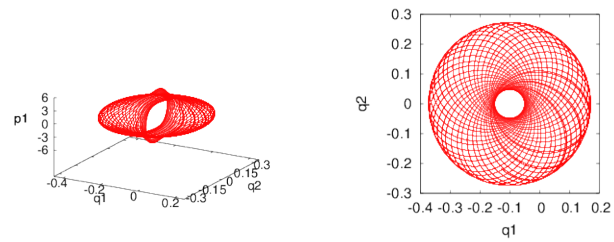

FIGURE 11. Two views of a two-dimensional quasiperiodic trajectory for the restricted three-body problem described in Section 4.2.

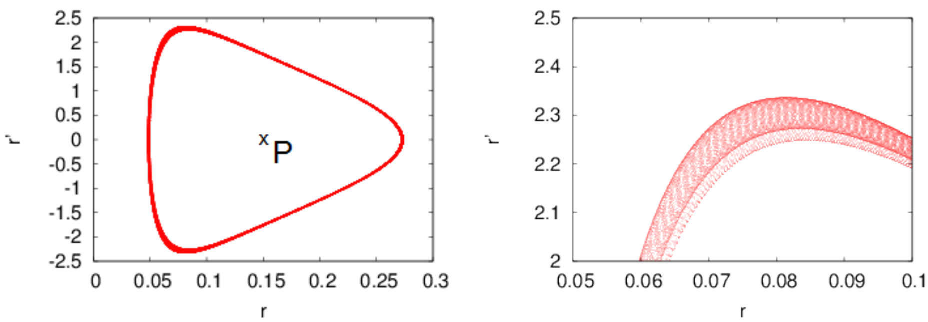

FIGURE 12. **Plots of the circular planar restricted three-body problem in $r - r'$ coordinates.** As described in the text, we define $r = \sqrt{(q_1 + 0.1)^2 + q_2^2}$ and $r' = dr/dt$. This figure shows r versus r' for a single trajectory. The right figure is the enlargement of the left. One of the two rotation rates ρ_ϕ^* is calculated by measuring from $(r, r') = (0.15, 0)$ in these coordinates.

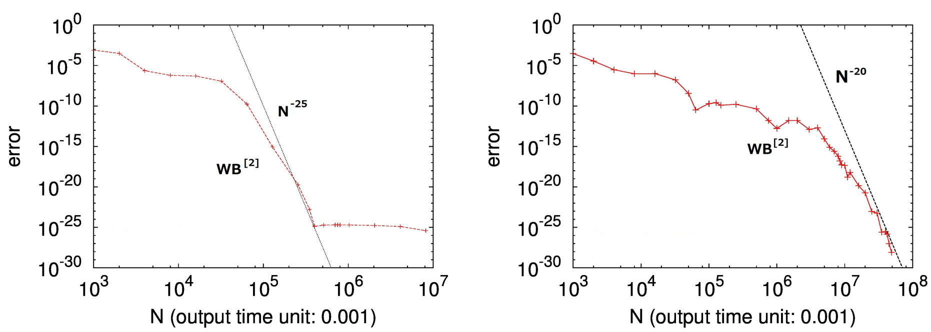

FIGURE 13. **Convergence to the rotation rates for the CR3BP.** For these two figures, we used differential equation time step $dt = 0.00002$ and we compute the change in angle after 50 such steps, that is, in time "output time" $Dt = 0.001$. We show the convergence rates to the estimated rate of $0.001 \times \rho_\theta^*$ (left) and of $0.001 \times \rho_\phi^*$ (right). For both cases rotation rates are calculated using the Weighted Birkhoff averaging method $\mathrm{WB}_N^{[2]}$ in Eq.13 and show fast convergence.

We measure angles as a fraction of a full rotation and not in terms of radians. The asteroid's orbit in rotating coordinates is shown in Fig. 11. Here time is continuous so we can measure the total angle through which a trajectory travels, retaining the integer part. The first rotation rate ρ^*_θ of the asteroid's orbit is its average rate of rotation about the planet, that is, the average rate of change of the angle θ measured from $(q_1, q_2) = (-0.1, 0)$. We compute that $\rho^*_\theta = -2.4978235048393444604083\,94$ rev/sec, that is, about -2.5 θ-revolutions per unit time Fig. 13 (left) shows the error in convergence to the value $0.001\rho^*_\theta$ Note that the rotation rate in the fixed coordinate frame is $\rho^*_\theta + 1/(2\pi)$.

The second rotation rate ρ^*_ϕ measures the oscillation in the distance r from the planet. In particular, we project to the (r, r') plane, where $r' := dr/dt$. That is, define $r = \sqrt{(q_1 + 0.1)^2 + q_2^2}$ and $r' = \frac{dr}{dt} = ((q_1 + 0.1)\frac{dq_1}{dt} + q_2\frac{dq_2}{dt})/r$, as shown in Fig. 12. The angle ϕ is measured from $(r, r') = (0.15, 0)$. The fast convergence to the value $0.001\rho^*_\phi$ by the Weighted Birkhoff Average $\mathrm{WB}^{[2]}_N$ in Eq. 13 is seen in Fig. 13 (right), where $\rho^*_\phi = -2.3380583953388194764236520190142509$ rev/sec. The period of time between perigees is the reciprocal, or about 0.43 time units.

We used the 8th-order Runge-Kutta method in Butcher [4] to compute trajectories of CR3BP with time steps of $h = 2 \times 10^{-5}$.

The meaning of rotation rates for the CR3BP. In [7], we investigated the same asteroid orbit of the CR3BP as is studied here, but instead of the continuous-time trajectory that lies on a two-dimensional torus as presented above, there we used a Poincaré map. The coordinates of the asteroid were recorded each time the asteroid crossed the line $q_2 = 0$ with $dq_2/dt > 0$. In the cases we study, the map trajectory is a quasiperiodic trajectory on a closed curve. Hence there is only one rotation rate, a much simpler situation. Choosing a point inside the closed curve, we computed a rotation rate, namely the average angular rotation *per iteration of the Poincaré map*. The rotation rate ρ^*_P per Poincaré map on the Poincaré surface $q_2 = 0$ (or equivalently, $\theta = 0$) around $(q_1, p_1) = (-0.25, 0)$ was computed as 0.06396172875745309716407772440144269 55. We felt that the issues of rotation rates could be clarified if we computed the trajectory as a continuous orbit as we do here. The two rotation rates computed here ρ^*_ϕ and ρ^*_θ and our previous result ρ^*_P bear the following relation to our previous results:

$$\rho^*_P = \left(\pm\frac{\rho^*_\phi}{\rho^*_\theta}\right) \bmod 1.$$

$$\rho^*_P = 0.06396\cdots = 1 - \frac{2.338\cdots}{2.497\cdots} \pm 10^{-25}$$

See the caption of Fig. 13. We solved the differential equation using an 8^{th}-order Runge-Kutta method using quadruple precision. Both approaches are based on rotating coordinates, but there is another approach.

The orbit as a slowly rotating ellipse. The asteroid rotates about the planet at a rate of ρ^*_θ revolutions per unit time when viewed in the rotating coordinate in which the moon and planet are fixed. The sidereal rotation rate (as viewed in the coordinates of the fixed stars) is $\rho^*_\theta\ + 1/(2\pi)$. We can think of the orbit as an approximate ellipse whose major axis rotates and even changes eccentricity (being more eccentric when the asteroid apogee is aligned with the planet moon axis).

Without the moon the asteroid orbit would be perfectly elliptical with its major axis fixed in position, but the moon causes the ellipse to rotate slowly. The angle

$\phi(t)$ tells where the asteroid is on its roughly elliptical orbit; Fig. 12 shows that the apogee occurs when when the distance from the planet $r \sim 0.27$ and the perigee when $r \sim 0.05$, with some variation. The time between successive perigees averages $1/\rho^*_\phi$. Note that the difference in these rates satisfies

$$\rho^*_\phi \ - [\rho^*_\theta \ + 1/(2\pi)] \sim 0.000610166 \sim 1/1638.9.$$

Hence relative to the fixed stars, that is, in non-rotating coordinates, the asteroid's ellipse's major axis precesses slowly. Its apogee point returns to its original position (in non-rotating coordinates) after the asteroid passes through its apogee approximately 1639 times.

5. **Discussion and conclusions.** What does it mean to ask for one or more rotation rates of the d-dimensional quasiperiodic map Eq. 1? One might expect that one should find ρ or rather its coordinates. As we explain below and in Section 2.2, this is an ill-posed problem (especially for $d > 1$. The Babylonians computed rotation rates for projections of the Moon's trajectory onto the globe of fixed stars (as we have discussed in the Introduction). So we refer to their approach as the "Babylonian Problem": computing rotation rates for a projection of a quasiperiodic process.

We have developed our Embedding continuation method for calculating the rotation rate for "almost every" Babylonian Problem, that is, for smooth projection ψ from of a quasiperiodic dynamical system on $\mathbb{T}^d$. "Almost every" is in the sense of prevalence - and in practice there will be difficult cases especially since the number N of interates needed increases as d increases. Our Weighted Birkhoff Method of computing rotation numbers significantly shortens the computation time for computing rotation numbers, making our approach effective in practice. See the Introduction.

A key motivating difference between $d = 1$ and $d > 1$ is that in the higher-dimensional case, for the rotation vector $\rho \in \mathbb{T}^d$ there are infinitely many ways of choosing coordinates on $\mathbb{T}^d$ for the map Eq. 1. In Section 2.2 we show that the set of resulting coordinate representations $(\rho_1, \cdots, \rho_d)$ of ρ are dense in $\mathbb{T}^d$. Every point r in $\mathbb{T}^d$ is arbitrarily close to such representations. Hence instead of trying to find the coordinates of ρ, we have learned from the Babylonians, and we phrase our goals in terms of finding a rotation number ρ_ψ (usually, ρ_ϕ or ρ_γ) for some projection from $\mathbb{T}^d$ into a one or two-dimensional space.

Even for $d = 1$, there is some uncertainty for obtaining ρ depending on the choice of orientation on S^1. We can obtain either $\rho \mod 1$ or $1 - \rho \mod 1$.

In Section 4.2, we apply our method to the quasiperiodic torus occurring for a 4-dimensional circular restricted 3-body problem, depicted in Fig. 11. In particular, we explain the relationship between the two rotation rates obtained from the original differential equation system and the rotation rate which was previously obtained from the Poincaré map. The fact that the rotation rate of an asteroid will be different depending on whether on uses rotating coordinates or sidereal coordinates (in which the distant stars are fixed) is an example of how the rotation rate can depend on the projection.

Notes on delay coordinate embedding theorems. H. Whitney [24] showed that a topologically generic smooth map Γ from a d-dimensional smooth compact manifold M into $\mathbb{R}^D$ where $2d+1 \leq D$ is a diffeomorphism on M; in particular the map $\Gamma : M \to F(M)$ is an embedding of M.

Sauer et al [21] modified Takens' result in two ways. First, it replaced "topologically generic" by "almost every" (in the sense of "prevalence") in Theorems 2.1

and 2.3 in [14]. See also [18]. For physical purposes "almost every" has significance while residual sets do not seem to. In this paper, in Theorem 1.2, we have adapted the "almost every" approach.

For completeness, we mention the second way [21] generalized Takens' approach, even though this second way is not used here, because the sets we deal with are manifolds. The second way is that [21] allblack replaced the assumption that M is a manifold by assuming only that $M \subset \mathbb{R}^k$ for some k is an invariant set of some map and that M has box dimension $boxdim(M)$ and Γ is a mapping of a neighborhood of M into $\mathbb{R}^D$ where $D > 2 \cdot boxdim(M)$. The great majority of citations to Takens [23] are for the case where M is a chaotic attractor that is not a manifold so that Takens' Theorem does not apply. Those papers actually use the results in [21], not in Takens' [23]. One unusual aspect of our current paper is that we actually only need the case that Takens proved. Here M is a quasiperiodic torus so it is a manifold.

The Takens Theorem also has assumptions that the set of periodic points $F : M \to M$ for some smooth map was in some sense small, in our case there are no periodic points so those assumptions are automatically satisfied. Hence we only state it in a special case needed here.

We have demonstrated that in one dimension, a rotation rate can be computed precisely with minimal ambiguity, but higher dimensional cases ($\mathbb{T}^d$ with $d > 1$) are more complicated. Projections into the plane yield rotation rates, but there are infinitely many topologically distinct ways to project a higher dimensional torus onto a circle, each of which yields a different rotation rate. This makes it important for the investigator to explain the meaning of any particular rotation rate. In fact, a rotation rate is a rate specifying an average change per unit time, where there can be considerable choice in the time units. To illustrate this point, we more carefully consider the CR3BP example with a focus on what the rotation rates tell us about the trajectories of an asteroid.

Acknowledgments. We would like to thank the referee for many helpful comments. YS was partially supported by JSPS KAKENHI grant 17K05360 and JST PRESTO grant JPMJPR16E5. ES was partially supported by NSF grant DMS-1407087. JY was partially supported by National Research Initiative Competitive grants 2009-35205-05209 and 2008-04049 from the USDA.

REFERENCES

[1] J. Barrow-Green, *Poincaré and the Three Body Problem*, Amer. Math. Soc., Providence, London, 1997.

[2] A. Belova, Rigorous enclosures of rotation numbers by interval methods, *J. of Comput. Dyn.*, **3** (2016), 81–91.

[3] M. Brin and G. Stuck, *Introduction to Dynamical Systems*, Cambridge University Press, 2002.

[4] J. C. Butcher, *Numerical Methods for Ordinary Differential Equations*, John Wiley & Sons, Ltd, Chichester, 2016.

[5] X. Cabré, E. Fontich and R. de la Llave, The parameterization method for invariant manifolds. I. Manifolds associated to non-resonant subspaces, *Indiana Univ. Math. J.*, **52** (2003), 283–328.

[6] S. Das, C. B. Dock, Y. Saiki, M. Salgado-Flores, E. Sander, J. Wu and J. A. Yorke, Measuring quasiperiodicity, *Europhys. Lett.*, **116** (2016), 40005.

[7] S. Das, E. Sander, Y. Saiki and J. A. Yorke, Quantitative quasiperiodicity, *Nonlinearity,* **30** (2017), 4111–4140,

[8] S. Das and J. A. Yorke, Super convergence of ergodic averages for quasiperiodic orbits, *Nonlinearity,* **31** (2018), 491–501,

[9] R. de la Llave, A. González, A. Jorba and J. Villanueva, KAM theory without action-angle variables, *Nonlinearity*, **18** (2005), 855–895.

[10] B. R. Goldstein, On the Babylonian discovery of the periods of lunar motion, *J. Hist. Astro.*, **33** (2002), 1–13.

[11] A. Haro and R. de la Llave, A parameterization method for the computation of invariant tori and their whiskers in quasi-periodic maps: explorations and mechanisms for the breakdown of hyperbolicity, *SIAM J. Appl. Dyn. Syst.*, **6** (2007), 142–207.

[12] B. Hasselblatt and A. Katok, Principal structures, in *Handbook of Dynamical Systems, North-Holland*, **1** (2002), 1–203.

[13] G. Huguet, R. de la Llave and Y. Sire, Fast iteration of cocycles over rotations and computation of hyperbolic bundles, *Discrete Contin. Dyn. Syst.*, 2013, 323–333.

[14] B. Hunt, T. Sauer and J. A. Yorke, Prevalence: a translation-invariant "almost every" on infinite dimensional spaces, *Bull. Amer. Math. Soc.*, **27** (1992), 217–238.

[15] J. Laskar, Introduction to frequency map analysis, in *Hamiltonian Systems with Three or More Degrees of Freedom(S'Agaró, 1995)*, vol. 533, Kluwer Acad. Publ., Dordrecht, 1999, 134–150.

[16] A. Luque and J. Villanueva, Numerical computation of rotation numbers of quasi-periodic planar curves, *Physica D*, **238** (2009), 2025–2044.

[17] A. Luque and J. Villanueva, Quasi-periodic frequency analysis using averaging-extrapolation methods, *SIAM J. Appl. Dyn. Syst.*, **13** (2014), 1–46.

[18] W. Ott and J. A. Yorke, Prevalence, *Bull. Amer. Math. Soc.*, **42** (2005), 263–290.

[19] H. Poincaré, *New Methods of Celestial Mechanics*, Translated from the French. NASA TT F-451 National Aeronautics and Space Administration, Washington, D.C., 1967.

[20] E. Sander and J. A. Yorke, The many facets of chaos, *Int. J. Bifurcat. Chaos*, **25** (2015), 1530011, 15pp.

[21] T. Sauer, J. A. Yorke and M. Casdagli, Embedology, *J. Stat. Phys.*, **65** (1991), 579–616.

[22] V. Szebehely, *Theory of Orbits: The Restricted Problem of Three Bodies*, Academic Press, Cambridge, MA, 1967.

[23] F. Takens, Detecting strange attractors in turbulence, in *Dynamical systems and turbulence, Warwick 1980 (Coventry, 1979/1980)*, vol. 898 of Lecture Notes in Math., Springer, Berlin-New York, 1981, 366–381.

[24] H. Whitney, Differentiable manifolds, *Annals of Math.*, **37** (1936), 645–680.

Received December 2016; revised July 2017.

E-mail address: iamsuddhasattwa@gmail.com
E-mail address: yoshi.saiki@r.hit-u.ac.jp
E-mail address: esander@gmu.edu
E-mail address: Yorke@umd.edu